Invited Paper

On the influx of small comets into Earth's atmosphere

L. A. Frank and J. B. Sigwarth

Department of Physics and Astronomy
The University of Iowa
Iowa City, IA 52242

ABSTRACT

Approximately 11 years ago unexpected transient decreases of Earth's dayglow intensities with spatial dimensions of approximately 50 km in diameter were detected in the first high-resolution global images from a high-altitude orbiting spacecraft, Dynamics Explorer 1. These decreases in dayglow intensities were measured in an ultraviolet spectral window that is very sensitive to absorption by water molecules and clusters along the camera's line-of-sight from the spacecraft to the sunlit atmosphere. These decreases exhibited several features that indicated an extraterrestrial source. Namely (1) preferential motion in the east-to-west direction across the sunlit face of Earth, (2) similar diurnal variations in occurrence rates as those for radar meteors, (3) correlation of the occurrence rates with the nonshower rates as determined with forward scatter radar, and (4) larger angular diameters for these atmospheric holes as the altitude of the spacecraft decreases. The only viable interpretation of these atmospheric holes to date is the impact of incoming water clouds from small comets that have disrupted in the vicinity of Earth. The startling consequence of this interpretation is an influx of about 20 small comets each minute into our atmosphere, each with a mass of tens of tons. These measurements and interpretation inspired a heated debate which resulted in dismissing the small comets because the observations were generally obtained at the imager's threshold. A new ultraviolet imager with more than 100 times the resolution of the Dynamics Explorer-1 camera has been recently flown on the Polar spacecraft. These images from the Polar camera confirm the existence of the small comets. A mission to further investigate the composition and dynamics of these small comets is suggested.

Keywords: small comets, atmospheric dayglow holes, extraterrestrial water

2. INTRODUCTION

A large influx of small comets into Earth's upper atmosphere was reported over a decade ago on the basis of transient decreases in Earth's far-ultraviolet dayglow as recorded in the images from the polar-orbiting, high-altitude spacecraft Dynamics Explorer 1.[1,2] The dayglow decreases were interpreted in terms of absorption along the camera's line-of-sight by water clouds from the small comets which disrupt at altitudes of 1000 to 2000 km and subsequently plunge into the upper atmosphere. Because most of these events, also known as "atmospheric holes", were seen in only one pixel of these dayglow maps the possibility that there was a large influx of small comets was not accepted (see overview by Dessler).[3] On the other hand, the atmospheric holes had been shown (1) to move in a preferential direction of east-to-west across the sunlit face of Earth, (2) to be observed with increasing apparent angular diameters as the spacecraft altitude decreased, (3) to have similar diurnal variations in occurrence rates as those for radar meteors, and (4) to exhibit occurrence rates which were correlated with those observed for nonshower meteor rates as detected with forward-scatter radar.[4] Still, the average global rates of about 20 impacts/minute and the individual comet masses of tens of tons were startling and have awaited confirmation with the next generation of dim-light imagers.

SPIE Vol. 3111 • 0277-786X/97/$10.00

3. SEVERAL CHARACTERISTICS OF ATMOSPHERIC HOLES

An example of a transient localized decrease in Earth's dayglow is shown in Figure 1. The diameters of these decreases are typically ~50–100 km and their durations are ~100 s or less. The principal dayglow emission is that of atomic oxygen at 130.4 nm. Because of the large diameters of the atmospheric holes and the fact that the above atmospheric emissions are strongly absorbed by water molecules, the only viable interpretation of these events to date is in terms of a flux of cometary water clouds into Earth's upper atmosphere. That is, the small comets are disrupted at altitudes in the range of 1000 to 3000 km, quickly vaporize, and produce an expanding cloud of water vapor which subsequently plunges into the atmosphere.

Figure 1. An atmospheric hole is shown in expanded view in the inset. The ring of emission at the top of this image is the northern auroral oval. This image was taken with a camera for far-ultraviolet wavelenghts on board the polar orbiting spacecraft Dynamics Explorer 1 at 1640 UT on 20 October 1981. The spacecraft position was located at an altitude of 18,500 km and geographic latitude and longitude of 41° and 242°, respectively [Ref. 1].

The interplanetary origins of these atmospheric holes are evidenced by their correlation with meteor rates. Frank et al.[5] are able to determine the temporal variations of the atmospheric hole rates for a fixed area of dayglow. This area, 1.1×10^7 km^2, is bounded by Earth–centered solar–ecliptic latitudes $30° \leq \theta_{SE} \leq 90°$ and longitudes $285° \leq \phi_{SE} \leq 315°$. The temporal variations of atmospheric hole rates for the period November 1, 1981, through January 21, 1982, in 2–day intervals are shown in the top panel of Figure 2. The averaged, daily meteor rates as determined with forward scatter radar from the same days but for different years are shown in the bottom panel of Figure 2.[6] We assume that the radar meteor rates are qualitatively similar from year to year. Periods of major showers are indicated by open circles and by closed circles for the nonshower periods. No evidence of increases of atmospheric hole rates during radar meteor showers are found in the figure. Instead, there is a remarkable correlation of the atmospheric hole rates with the nonshower, or sporadic, radar meteor rates. The reader should note the remarkable correlations

between the atmospheric hole rates and the nonshower radar–meteor rates shown in Figure 2, for example, (1) the overall decrease in meteor rates by a factor of ~10 over the period November 1 to mid–January, (2) the decrease in rates on about November 8, (3) the increase in rates on about November 30, (4) the period of more or less constant rates during December 20 to January 6, and (5) the minimum in event rates in mid–January with subsequent recovery. The weakly bound small comets and mantle debris are expected to produce ionization at higher altitudes relative to that from stony or iron meteoroids. Forward scatter radar is much more sensitive to ionization at higher altitudes relative to backscatter radar stations.[7] Thus the correlation of atmospheric hole rates with those of radar meteors is expected in forward scatter, whereas backscatter radar events are dominated by the infall of iron and stony meteoroids.

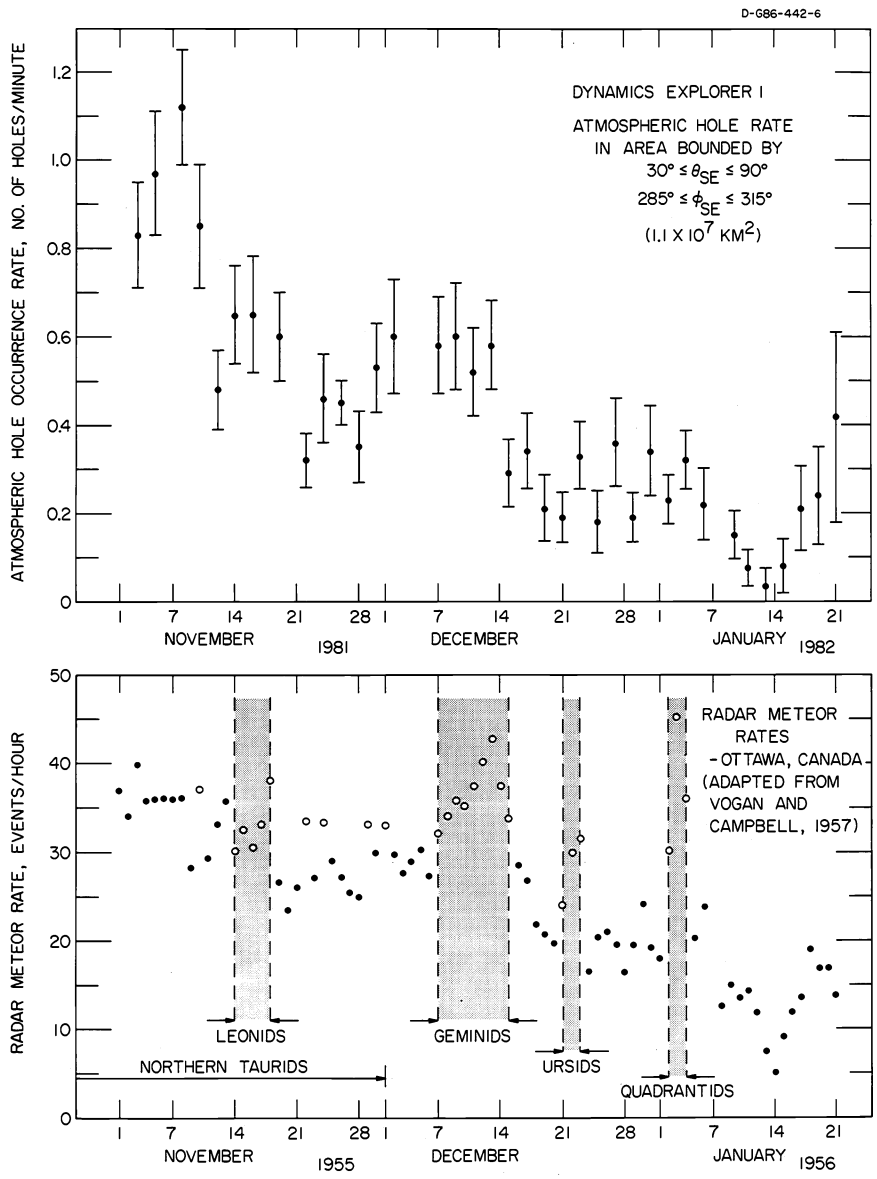

Figure 2. (Upper panel) Average occurrence rates of atmospheric holes during the period November 1981 through late–January 1982. (Lower panel) Forward scatter meteor rates reported by Vogan and Campbell [1957] for the same months but for earlier years 1955 and 1956 [Ref. 5].

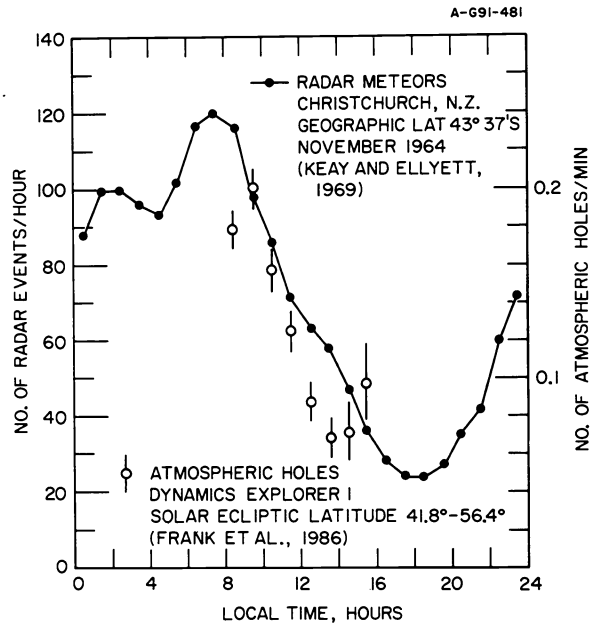

Figure 3. Comparison of the diurnal variations of the rates of atmospheric holes and radar meteors at mid-latitudes. The occurrence rates for atmospheric holes are given for an area of 1.8×10^6 km^2 [Ref. 1].

The diurnal variations of the rates of atmospheric holes as given by Frank et al.[1] are shown in Figure 3. Of course, atmospheric hole rates cannot be determined for nighttime. The meteor rates from a ground-based, backscatter radar station are also shown in Figure 3 for an appropriate latitude.[8] The diurnal variations as determined with forward scatter radar are similar.[6] The agreement between the diurnal variations for atmospheric holes and radar meteors is obviously good.

One of the interesting issues for the low-altitude disruption of these small comets is the fact that the mechanism becomes very effective in the altitude range of about 1000 to 3000 km. This is a relatively constrained range in consideration of their transport through interplanetary space.

The atmospheric ram pressures at altitudes ~1000 km are ~10^{-5} dyne/cm^2 and are probably too small for disruption of the small comets. The tidal stresses at these altitudes, ~0.1 dyne/cm^2, are in the range of the water vapor pressures constrained by the mantle. However, the radial dependence of these tidal stresses varies as r^{-3}, where r is the geocentric radial distance and does not yield a rapid increase in stress over altitudes of 1000 to 3000 km. Of the three disruptive forces originally identified by Frank et al.,[2] electrostatic forces appear to be the most likely mechanism for removal of the protective mantle at altitudes ~1000 km.

The electrostatic stress on a smooth sphere with diameter of 12 m and a potential of $V_0 = 10$ V is shown in Figure 4 as a function of altitude above the Earth's surface. This value for V_0 is chosen because it is scalewise representative of the potential due to $-\mathbf{V} \times \mathbf{B}$ electric fields at the ionospheric altitudes, which are of primary interest here. The stress is $|\mathbf{E}_0|^2/8\pi$, where $\mathbf{E}_0$ is the electric field at the mantle surface. At altitudes beyond the plasmasphere the electrostatic screening thickness, or Debye length λ_D, in the ambient plasma is large relative to the radius R_0 of the small comet and thus $|\mathbf{E}_0| \simeq V_0/R_0$. As λ_D decreases with decreasing altitude inside of the plasmapause, $|\mathbf{E}_0| \simeq V_0/\lambda_D$. Representative values for λ_D are taken from Garrett[9] and combined with altitude profiles of plasma densities in the plasmasphere[10] and in the ionosphere[11] in order to calculate the electrostatic stress on the mantle surface shown in Figure 4. On the basis of the altitude profile of these electrostatic forces we find that there is a planet-wide, large increase in the electrostatic forces at altitudes $<$ 1000 to 3000 km. We use these values for the breakup altitude.

The electrostatic stresses on the comet as shown in Figure 4 are minimum values derived with the assumptions of a smooth exterior surface for the mantle of the small comet. It is not unreasonable to assume that the heights and lateral dimensions of the surface topology exhibit irregularities on scales of ~1% of the diameter of the object, i.e., ~10 cm. When λ_D is large, for example, in the outer magnetosphere and solar wind, the electrostatic stresses can be expected to increase only by factors in the range of 10 at most relative to smooth-surface values.[12]

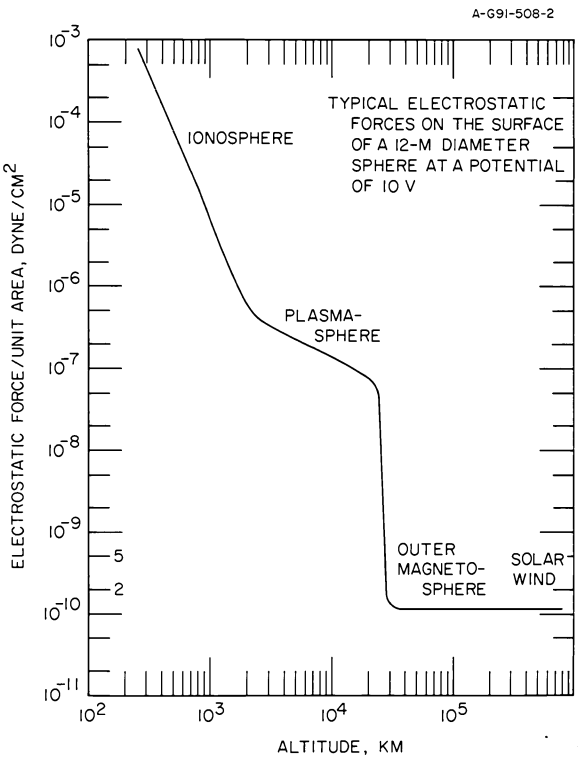

Figure 4. Typical electrostatic forces per unit area on the surface of a smooth sphere with radius 6 m and at a potential of 10 V as a function of altitude above the dayside surface of Earth. A steep gradient in these forces with decreasing altitude occurs at about 1000 to 2000 km [Ref. 4].

On the other hand, as the small comet enters the ionosphere at altitudes of ~1000 km the Debye sheath rapidly collapses in thickness. For example, the Debye length λ_D is only ~5 cm at 1000 km and protrusions from the mantle surface are likely to extend beyond the sheath. The calculation of the expected electric fields on these protrusions is not straightforward: extensive numerical modeling is required. In a conceptual sense we suggest that the outer boundary of the Debye sheath can be treated as a ground plane with respect to the ambient plasma and that the maximum electric fields on the charged protrusions are characterized by their radii for points and edges. For example, the electrostatic stresses for such radii of 10^{-2} and 10^{-3} cm are ~0.4 and 40 dyne/cm^2, respectively. These stresses are factors ~3×10^5 and 3×10^7 greater than those of a smooth sphere at an altitude of 1000 km. If such electrostatic forces are yielded by the collapse in Debye sheath thickness then a rapid erosion of the mantle material could be expected with subsequent destruction of the integrity of the mantle and disruption of the cometary core. An appropriate analogy may be the action of sandpaper on the surface of a gas-filled balloon.

4. NEW OBSERVATIONS OF SMALL COMETS

On 24 February 1996 the Polar spacecraft was launched into an eccentric orbit with perigee and apogee altitudes of 5170 km and 50,510 km, respectively, an orbital period of 17.6 hours, and an inclination of 86°. This spacecraft was equipped with a despun platform which allows the Visible Imaging System (VIS) to stare at Earth. The VIS is composed of three cameras, the Earth Camera for far-ultraviolet auroral and dayglow emissions, primarily those of OI 130.4 nm, and two cameras for visible wavelengths, the Low-Resolution Visible Camera and the Medium-Resolution Visible Camera.[13] These cameras for visible wavelengths are serviced with a filter wheel with twelve individual filters. Of present interest is the filter at 308.5 nm with centered passband width of 5.6 nm. This filter is sensitive to the solar resonance fluorescence from the OH radical in the (0, 0) band of $A^2\Sigma^+ - X^2\Pi$. Images from the Low-Resolution Visible Camera are presented here. The field-of-view of this camera is 5.4° × 6.3° and is serviced by an intensified charge-coupled device (CCD). The CCD provides an array of 256 × 256 picture elements (pixels), each with field-of-view of about 0.02° × 0.02°. The fields-of-view of the visible cameras could be placed at any position within a field-of-view of 20° × 20° via a mirror which is pointed with a bi-axial motor drive.

A severe complication arose in the operation of the VIS when it was found after launch that the spacecraft center-of-mass could not be positioned onto the spin axis of the spacecraft with the onboard movable masses. The major portion of the spacecraft is intentionally spinning with a period of 6 s in order to accommodate the fields-and-particles instrumentation. The inability to balance the spacecraft mass produced a cyclic motion of the angular pointing of the platform with amplitude

of 0.38° and period of 6 s. The projection of this circular motion onto the image planes of the cameras produced two bright ansae. An example of this effect can be found for the Earth Camera as reported by Frank and Sigwarth.[14] For the Low–Resolution Visible Camera the corresponding amplitude of this undesired motion is 19 pixels, and insufficient for resolving the cometary water clouds. The expected apparent angular dimensions are in the range of one to several pixels. Hence the instrument's onboard computers were reprogrammed to sample only one of the two bright ansae and thus restore the angular resolution of the camera. The instrument was already programmed to electronically shutter the sensors when the long booms and antennas of the spacecraft enter the cameras' fields–of–view for relatively brief intervals during the spacecraft rotation. Of course, the sampling time was now severely reduced to 1 s during each spacecraft rotation of 6 s with a corresponding loss of sensitivity. However, as will be apparent in the images presented here, the sensitivity is adequate to detect the cometary OH emissions.

An example of the detection of the OH trail due to the motion of a cometary water cloud is given in Figure 5.[15] There are three detections shown in this frame for the following reason. The total sampling period is 13.5 s and is composed of three brief snapshots of 1 s each. For an object with constant apparent speed the three detections must be collinear, have equal separations and be of very similar magnitudes. This is a marvelously simple and constrained method of separating these sightings from the source of image contamination, i.e., the deposition of charge due to the

Figure 5. Three consecutive snapshots of the OH emissions at 308.5 nm which are associated with the motion of a cometary water cloud above Earth's atmosphere. These snapshots were taken at 0451 UT on 31 December 1996 with a camera for visible wavelengths on board the recently launched Polar spacecraft. An image of Earth has been superposed onto the three snapshots for the purpose of providing the perspective for the snapshots relative to our planet because there are no detectable emissions from the nighttime atmosphere or surface at this wavelength [Ref. 15].

penetration of energetic charged particles in the sensor. This method was verified by interleaving images with filters at other wavelengths. No trails were detected in these latter images. The field–of–view shown in Figure 5 matches that of the actual image. The Earth is viewed only at nighttime because viewing the enormous intensities of the dayside would quickly destroy the sensor. The OH intensities in Earth's nighttime atmosphere are generally below the sensitivity of the camera. In order to provide orientation and perspective for the image a simulation of the actual geographical features at the time of the image has been superposed on the light trail. The geographical image is generated by the software FACE OF THE EARTH™ (copyright © 1996, ARC Science Simulations). The apparent angular speed of the trail is 0.06°/s.

The Low–Resolution Visible Camera on board the Polar spacecraft was successfully employed to detect the trails of OH radicals at 308.5 nm which are due to the presence of cometary water clouds at altitudes in the range of 3000 km or less above Earth's surface. The OH radicals are presumably due to the photodissociation of water by solar radiation and/or the direct release from the water snow as it vaporizes. As a benchmark in the evolution of auroral and dayglow imagers it is noted that the resolution of the above camera for visible wavelengths provides about 155 pixels within the solid angle for a single pixel of the Dynamics Explorer–1 images. Such advances in instrumentation are necessary for obtaining the first images of the OH trails as reported in the present paper. These OH emissions are due to resonance fluorescence from the solar radiation. This, together with the fact that the wavelength is near the ultraviolet edge of the atmospheric transmission window, will make the dim trail very difficult, if not impossible, to be observed with the unaided eye of a ground observer.

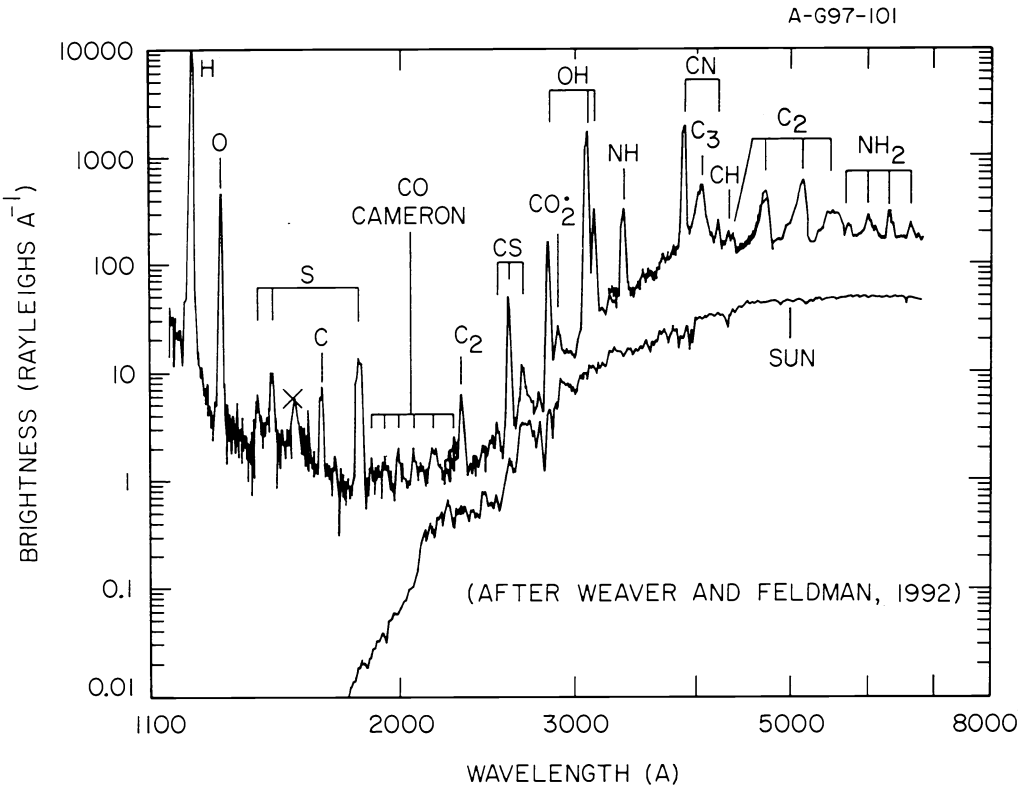

Figure 6. A composite spectrum of P/Hartley 2 (1991 XV) spanning the wavelength range from HI Ly–α to 7000 Angstroms as taken with the Faint Object Spectrograph (FOS) of the Hubble Space Telescope (HST) [Ref. 16].

5. BASELINE OPTICS FOR FUTURE MISSIONS

The cameras on board the Polar spacecraft were optimized for studies of Earth's auroras. Only a few of the optical filters in these cameras were relevant to cometary emissions. A camera devoted to studies of the water clouds from the breakup of small comets at low-altitudes should accommodate a selection of the emissions from large, well-known comets as a guideline. Figure 6 shows a spectrum for P/Hartley 2.[16] Prominent emissions include those from oxygen, CS, OH, CN and NH_2, for examples.

The camera for a future mission devoted to the investigations of the small comet influx into our atmosphere should have a large field-of-view and a sensitivity that will allow high-speed (a few seconds or less) frame sequences of the evolution of a cometary water cloud. The Earth Camera of the Polar spacecraft offers such a capability with a few modifications. An overview of the Polar Earth Camera and its sensor is provided here.

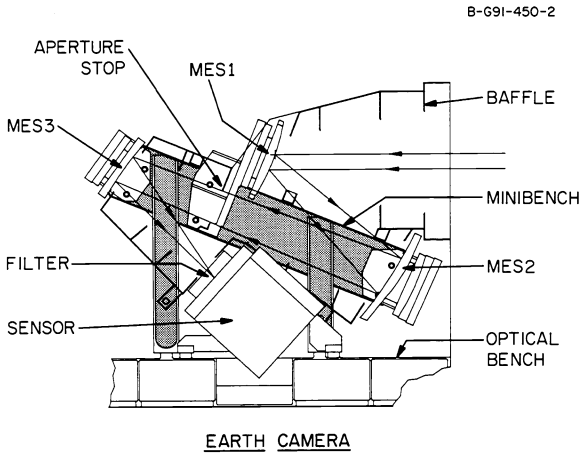

Figure 7. Diagram of the optics for the Earth Camera for the Polar spacecraft. This camera has the large field-of-view and sensitivity which are required to record the cometary water clouds at low altitudes [Ref. 13].

The optics of the Earth camera consists of three off-axis mirrors.[13] This design is based upon a similar camera previously described by Hallam et al.[17] The present optics provides a speed of f/4.6 with an entrance pupil diameter of 0.85 cm. The field-of-view of the Earth camera is 20° × 20°. A diagram of the mechanical configuration of the Earth sensor is shown in Figure 7. A list of the mirror parameters is given in Table I. The image at the sensor is provided by a convex spherical mirror MES1, an off-axis parabolic mirror MES2 and a concave spherical mirror MES3, in order of their appearance along the optical path. An ultraviolet transmission interference filter with peak transmission at 130 nm is placed in front of the sensor. The half-maximum full-width of the passband is 25 nm. It is this filter that will be replaced with a wheel with 12 filters for the observations of the small comets.

Table I. Optical Elements of the Earth Camera

Mirror, (Description)	Area, cm^2	Radius, r, cm	Focal Length, cm	Off-Axis Distance, H, cm
MES1 (Spherical Convex)	15.2	2.2	-6.515	---
MES2 (Off-Axis Parabola)	26.4	2.9	12.917	3.996
MES3 (Spherical Concave)	11.3	1.9	11.794	---

A diagram of the sensor assembly is shown in Figure 8.[13] The image intensifiers are based in large part on the design for commercial generation–II 25–mm devices. In order to increase the photocathode lifetime a thin film of SiO_2 is deposited over the front face of the microchannel plate (MCP) assembly. This assembly consists of two MCPs in the chevron configuration. The photocathode for the visible cameras is trialkali type S20 and that for the Earth camera is cesium iodide. The trialkali photocathode will be substituted into the Earth Camera for the investigations of small comets. The output electrons from the MCPs are proximity–focused into a phosphor, JEDEC registration GH. The wavelength for the phosphor spectral maximum is 525 nm. The decay times for the phosphor emissions after shuttering the light source to the sensor are ~250 μs and 1s for decreases by factors of 10^{-2} and 10^{-3}, respectively. The image intensifiers were manufactured by Science Applications International Corporation at San Diego and the MCPs were supplied by Galileo Electro–Optics Corporation. The overall amplification of the light input is in the range of 10^5 and is determined by the potential differences across the MCP assembly and between the MCP output face and the phosphor. These bias voltages are controlled by ground command and can be selected to values of 0 to 2500 V and 0 to 5700 V, respectively. The gain of the image intensifier is sufficient to allow single–electron events at the entrance aperture of the MCP to be recorded by the CCD. The photocathodes can be back–biased in order to prevent current surges in the MCPs due to an extremely bright light source or to eliminate the effects of stray light from the science antennas that are mounted on the spinning section of the spacecraft and hence periodically appear within the fields–of–view of the cameras. This electronic shutter can be activated by an alarm from the MCP current monitor and by spin phase information from the spacecraft that is processed by the instrument electronics.

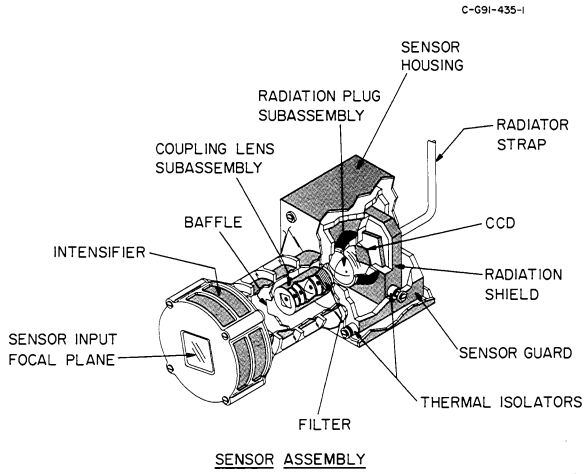

Figure 8. Cut–away diagram of the sensor assembly which is used for dim–light imaging by the cameras on the Polar spacecraft [Ref. 13].

The image on the phosphor at the exit face of the intensifier is transferred to the CCD by a coupling lens assembly. A series of baffles prevents significant stray light scattering from the phosphor into the CCD (see Figure 8). A wideband transmission filter is mounted on the back of the coupling lens subassembly in order to limit chromatic aberration to acceptable values. The center of the filter passband and the passband width at half–maximum transmissions are 530 (±25) nm. The coupling lenses are followed by a radiation plug subassembly, a 2–cm thick meniscus lens that can be mechanically translated along the chief ray for image focusing at the CCD.

The CCD is a Photometrics model PM516A which is manufactured by the Loral–Fairchild Imaging Sensors Group. This device has a pixel size of 20μm × 20μm with a 2–μm channel stop. The array size is 512 × 512 pixels. The baseline operating mode sums a block of 2 × 2 pixels to yield one pixel. The design of the CCD electronic controller is centered upon a custom–made type–8000 gate array fabricated by United Technologies Microelectronics Center.

In summary an effective camera for visible wavelengths with filter passbands selected for cometary emissions can use the Earth Camera on the Polar spacecraft for baseline optics and sensor design. A tremendous advantage for viewing the cometary water clouds would be a circular orbit at low altitudes, ~1000 km. Recall that the sightings with the Polar spacecraft were gained from much higher altitudes, $\gtrsim$ 10,000 km. In the low–altitude orbit, a detection of a cometary water cloud would occur every 10 minutes on the average if the camera's field–of–view and range were 20° × 20° and 4000 km, respectively.

ACKNOWLEDGMENTS

The snapshots of the cometary water clouds were superposed onto FACE OF THE EARTH™ (copyright © 1996, ARC Science Simulations). This research was supported in part at The University of Iowa by NASA Contract NAS5–30316.

REFERENCES

1. Frank, L. A., J. B. Sigwarth and J. D. Craven, On the influx of small comets into the Earth's upper atmosphere, I. Observations, *Geophys. Res. Lett., 13,* 303–306, 1986.

2. Frank, L. A., J. B. Sigwarth and J. D. Craven, On the influx of small comets into the Earth's upper atmosphere, II. Interpretation, *Geophys. Res. Lett., 13,* 307–310, 1986.

3. Dessler, A. J., The small comet hypothesis, *Rev. Geophys., 29,* 355–382, 1991.

4. Frank, L. A. and J. B. Sigwarth, Atmospheric holes and small comets, *Rev. Geophys., 31,* 1–28, 1993.

5. Frank, L. A., J. B. Sigwarth and J. D. Craven, Reply to Soter, *Geophys. Res. Lett., 14,* 164–167, 1987.

6. Vogan, E. L. and L. L. Campbell, Meteor signal rates observed in forward–scatter, *Can. J. Phys., 35,* 1176-1189, 1957.

7. McKinley, D. W. R., *Meteor Science and Engineering,* McGraw–Hill, New York, 1961.

8. Keay, C. S. L. and C. D. Ellyett, Southern hemisphere meteor rates, *Mem. R. Astron. Soc., 72,* 185–232, 1969.

9. Garrett, H. B., The charging of spacecraft surfaces, *Rev. Geophys., 19,* 577–616, 1981.

10. Horwitz, J. L., R. H. Comfort and C. R. Chappell, A statistical characterization of plasmasphere density structure and boundary locations, *J. Geophys. Res., 95,* 7937–7947, 1990.

11. Banks, P. M. and G. Kockarts, *Aeronomy, Part A,* p. 13, Academic, San Diego, Calif., 1973.

12. Harnwell, G. P., *Principles of Electricity and Electromagnetism,* problem 12, p. 79, McGraw-Hill, New York, 1949.

13. Frank, L. A., J. B. Sigwarth, J. D. Craven. J. P. Cravens, J. S. Dolan, P. K. Hardebeck, J. D. Harvey and D. Muller, The visible imaging system (VIS) for the Polar spacecraft, *Space Sci. Rev., 71,* 297–328, 1995.

14. Frank, L. A. and J. B. Sigwarth, Transient decreases of Earth's far–ultraviolet dayglow, *Geophys. Res. Lett.,* (submitted for publication), 1997.

15. Frank, L. A. and J. B. Sigwarth, Trails of OH emissons from small comets in the vicinity of Earth, *Geophys. Res. Lett.,* (submitted for publication), 1997.

16. Weaver, H. A. and P. D. Feldman, Probing the Nature of Comets with the Hubble Space Telescope, in *Science with the Hubble Space Telescope,* eds. P. Benvenuti and E. Schreier, ESO, p. 475, Garching, Germany, 1992.

17. Hallam, K. L., B. J. Howell and M. E. Wilson, An All-Reflective Wide-Angle Flat-Field Telescope for Space, in *Instrumentation in Astronomy V,* eds. A. Boksenberg and D. L. Crawford, Proceedings of SPIE, V. *445*, pp. 295–300, London, England, 1983.

Further author information -
L. A. F. (correspondence): Email: frank@iowasp.physics.uiowa.edu; WWW: http://www-pi.physics.uiowa.edu/; Telephone: 319-335-1695; Fax: 319-335-1753
J. B. S. Email: sigwarth@iowasp.physics.uiowa.edu; Telephone: 319-335-1867; Fax: 319-335-1753